Lithium extraction from shale gas flowback and produced water using H1.33Mn1.67O4 adsorbent

In preparation for ***Resources, Conservation and Recycling***

Date: March 21, 2022

Lithium Extraction from Shale Gas Flowback and Produced Water Using $H_{1.33}Mn_{1.67}O_4$ Adsorbent

Lun Tian [a, b], Yuanhui Liu [a, b], Peng Tang [a, b], Yushun Yang [a, b], Xingrui Wang [c], Tianxin Chen [c], Yuhua Bai [d], Alberto Tiraferri [e], Baicang Liu [a, b, *]

[a] Key Laboratory of Deep Earth Science and Engineering (Ministry of Education), Institute for Disaster Management and Reconstruction, Institute of New Energy and Low-Carbon Technology, College of Architecture and Environment, Sichuan University, Chengdu, Sichuan 610207, PR China

[b] Yibin Institute of Industrial Technology, Sichuan University Yibin Park, Section 2, Lingang Ave., Cuiping District, Yibin, Sichuan 644000, PR China

[c] Petro China Southwest Oil & Gasfield Company, No.5 Fuqing Rd., Chengdu, Sichuan 610051, PR China

[d] Infrastructure Construction Department, Chengdu University, Chengdu, Sichuan 610106, PR China

[e] Department of Environment, Land and Infrastructure Engineering, Politecnico di

[*]Corresponding author. Tel.: +86-28-85995998; fax: +86-28-62138325; E-mail: bcliu@scu.edu.cn; baicangliu@gmail.com (B. Liu).

Torino, Corso Duca degli Abruzzi 24, 10129 Turin, Italy

Abstract: The rapid growth of demand for lithium, especially in lithium batteries calls for an increase in the supply of lithium resources. We synthesized $H_{1.33}Mn_{1.67}O_4$ adsorbent by solid-phase reaction method to recover lithium for the first time from shale gas flowback and produced water (SGFPW) in the Sichuan Basin, China. In order to improve the adsorption capacity and selectivity of lithium, Na_2CO_3 precipitation pre-treatment was employed to remove some divalent ions (Ca^{2+}, Ba^{2+}, Sr^{2+}, Mg^{2+}) and to increase the pH prior to lithium adsorption. The adsorption capacity of lithium in the pre-treated water (P-SGFPW) was 16.2 mg/g higher than that in SGFPW (13.3 mg/g), and the partition coefficient of Li^+ increased from 731.6 to 1074mL/g after precipitation. After four cycles of adsorption and desorption, the adsorption capacity of lithium was stable and showed only a slight decrease equal to 3.53% and 5.35% in P-SGFPW and SGFPW, respectively. $H_{1.33}Mn_{1.67}O_4$ is a promising adsorbent for lithium extraction from SGFPW, and precipitation before adsorption can improve its performance significantly.

Keywords: Lithium recovery; Hydrogen manganese oxide ($H_{1.33}Mn_{1.67}O_4$); Adsorption; Shale gas flowback and produced water (SGFPW); Precipitation

1. Introduction

Lithium is regarded as “the energy metal of the 21st century” and “the white oil of the future” and may be as precious as gold (Tarascon, 2010). Lithium is one of the most electrochemically active metals, and it is a solid element with the highest redox potential, the largest specific heat capacity, the smallest density, the lightest weight, and the highest energy density at room temperature (Miatto et al., 2021; Swain, 2017; Zhang et al., 2021a). Therefore, lithium is widely used in various high-value products, such as batteries, ceramics, glass, in the nuclear industry, medicine, aerospace (Draaisma, 2019; Sun et al., 2021; U. S. Geological Survey, 2022; Zhang et al., 2021b). For example, electric vehicles and portable electronic devices deploy lithium batteries due to their high energy density, long service life, and relative environmental friendliness (Scrosati et al., 2011; Xie and Lu, 2020). The rapid development of the electric vehicle industry under the global “dual carbon” goal has led to a sharp increase in the demand for lithium batteries, with the proportion of lithium batteries in the global end-use markets increasing from 27% in 2011 to 74% in 2021 (U. S. Geological Survey, 2012, 2022). Global lithium consumption is estimated to be 93,000 tons in 2021, an increase of 33% from 70,000 tons in 2020, but lithium production (excluding U.S. production) only increased 21% (U. S. Geological Survey, 2022).

At present, lithium resources are mainly distributed in ores, seawater, and brines, e.g., oilfield brines, continental brines, geothermal brines (Swain, 2017). Extraction of

lithium from ores require cumbersome steps and has significant environmental impacts, including water pollution, soil pollution, and air pollution due to the use of copious quantities of chemicals, as well as the production of substantial amounts of acidic wastewater and solid waste (Hou et al., 2021; Yang et al., 2018). The total mass of lithium in seawater is abundant, but its concentration is very low (0.17 mg/L), making its selective extraction challenging from this source. Extraction of lithium from continental brines in China, Chile, and Argentina has been studied and widely applied, but oil and gas produced water is still an untapped lithium resource (Hou et al., 2021). Lithium concentrations in Marcellus shale gas flowback and produced water (SGFPW) ranges from 4 to 202 mg/L, and the median lithium concentration in SGFPW in the Sichuan Basin is 33 mg/L (Haluszczak et al., 2013; Xie et al., 2022). Horizontal drilling and hydraulic fracturing technologies have promoted the large-scale exploitation of shale gas, but they produce a large amount of FPW (Tang et al., 2022). It is estimated that the volume of SGFPW will reach 499-3585 million m^3 globally and 50-73 million m^3 in China by 2030 (Kondash et al., 2018; Liu et al., 2022). SGFPW is a potential resource for lithium recovery, and recovery of lithium from this wastewater as a secondary raw material would not only ease the imbalance between supply and demand, but also offset part of the cost of shale gas wastewater treatment by creating new value for this resource in the framework of circular economy (Kumar et al., 2019; Robbins et al., 2022). However, suitable and commercially feasible technologies for lithium recovery from SGFPW needs to be

improved.

Currently, there are several technologies for lithium recovery from solution, including precipitation (Zhang et al., 2019), extraction (Xiong et al., 2022), adsorption based on aluminum-based adsorbents ($LiCl{\cdot}2Al(OH)_3{\cdot}nH_2O$) (Zhong et al., 2021), manganese-based adsorbents (HMn_2O_4 (Han et al., 2020), $H_{1.33}Mn_{1.67}O_4$ (Seip et al., 2021), $H_{1.6}Mn_{1.6}O_4$ (Su et al., 2022)) and titanium-based adsorbents (H_2TiO_3 (Zhu et al., 2021), $H_4Ti_5O_{12}$ (Zhao et al., 2021)), as well as membrane-based methods, such as nanofiltration (Wang et al., 2021), electrodialysis (Chan et al., 2022), bipolar membranes electrodialysis (Bunani et al., 2017), membrane capacitive deionization (Shi et al., 2019), forward osmosis (Sutijan et al., 2022), electrochemical methods (Jang et al., 2021) and other hybrid techniques like reverse osmosis-electrodialysis (Qiu et al., 2019) or nanofiltration-membrane distillation (Pramanik et al., 2019)). Among these technologies, adsorption is one of the most promising methods for recovering lithium from oil and gas produced water due to minimal required pretreatment, low environmental impact, and high recovery efficiency (Safari et al., 2020).

Aluminum-based adsorbents are currently the only adsorbents used in industry, but their adsorption capacities are low (Sun et al., 2021). According to the research results discussed by Chen *et al*., when the ratio of the adsorbent to brine is 1 g/30 mL, the equilibrium adsorption capacity of the aluminum-based adsorbent is only roughly 7.1 mg/L (Chen et al., 2020). Alternative options are $H_{1.6}Mn_{1.6}O_4$ and $H_4Ti_5O_{12}$, which

however cannot be directly synthesized by solid phase reaction method, and intermediate products $LiMnO_2$ and $LiTi_2O_3$ need to be synthesized first, respectively. The temperature required for the synthesis of HMn_2O_4 and HTi_2O_3 by the solid phase reaction method is high, as these materials are typically calcined at 800 ℃ for 5 h (Ji et al., 2017) and 700 ℃ for 4 h (Lawagon et al., 2019), respectively, while $H_{1.33}Mn_{1.67}O_4$ only needs 4 h at 500 ℃ (Tang et al., 2020). In fact, $H_{1.33}Mn_{1.67}O_4$ is by far the most convenient adsorbent to synthesize among those discussed above. Moreover, due to its high chemical stability, high adsorption capacity, high selectivity, low toxicity, and low cost (Xu et al., 2019), $H_{1.33}Mn_{1.67}O_4$ is surely one of the most promising adsorbents for lithium recovery from SGFPW.

This is the first study of lithium recovery from SGFPW in the Sichuan Basin, China. In this study, we synthesize $Li_{1.33}Mn_{1.67}O_4$ precursor by solid phase reaction method and obtain the $H_{1.33}Mn_{1.67}O_4$ adsorbent by pickling with HCl. Then, we evaluate the feasibility of $H_{1.33}Mn_{1.67}O_4$ applied to lithium recovery from SGFPW by adsorption kinetics, adsorption isotherm, adsorption selectivity, and reusability. We also investigate the effect of pH values and pre-treatment by Na_2CO_3 precipitation on lithium recovery from the SGFPW. The results are supported by in-depth determination of physical and chemical properties of the $H_{1.33}Mn_{1.67}O_4$ adsorbent.

2. Materials and methods

2.1. Materials

The SGFPW used in the experiment was collected from a shale gas well, which

is located in Gongxian, Sichuan Basin, China, in the Lower Silurian Longmaxi Formation, as described in our previous work (Tian et al., 2020). The collected SGFPW samples were stored in plastic buckets under dark conditions before experiments. Lithium carbonate (Li_2CO_3), manganese carbonate ($MnCO_3$), sodium carbonate (Na_2CO_3), hydrochloric acid (HCl), sodium hydroxide (NaOH) were purchased from Kelong Chemical (Chengdu, China). All chemicals used in the experiments were of analytical grade. Ultrapure water with a resistivity of 18.25 MΩ was obtained from an ULURURE ultrapure water machine (Chengdu, China).

2.2. Preparation of the $H_{1.33}Mn_{1.67}O_4$ adsorbents

Li_2CO_3 and $MnCO_3$ were mixed and ground uniformly at a Li/Mn mole ratio of 1.33:1.67. The mixture was placed in a ceramic boat and calcined at 500 ℃ for 4 h in a muffle furnace in ambient air at a ramping rate of 3 ℃/min, and then cooled to room temperature. The product obtained was $Li_{1.33}Mn_{1.67}O_4$ (LMO). In order to obtain the $H_{1.33}Mn_{1.67}O_4$ (HMO) adsorbent, 1 g LMO was added to 1 L of 0.5 mol/L HCl and stirred at 200 rpm for 24 hours for delithiation. Finally, the adsorbents were washed with ultrapure water, filtered, and then dried at 50 ℃ for 24 h.

2.3. Characterization of $H_{1.33}Mn_{1.67}O_4$ adsorbents

The surface morphology and element electron binding energy were measured by field-emission scanning electron microscopy (FE-SEM) (Regulus-8230, Hitachi, Japan) and X-ray photoelectron spectroscopy (XPS) (AXIS Supra, Kratos, U.K.), respectively. Powder X-ray diffraction (XRD) patterns were recorded on a DX-2700

(Dandong Haoyuan, China) instrument equipped with a Cu Kα radiation (k = 0.15418 nm) in the 2θ range of 10°-80°; the step size of 0.05° and accumulation time of 0.5 s were adopted during scanning. N_2 adsorption-desorption isotherms were measured at the temperature of liquid N_2 (77 K) using an ASAP 2460 analyzer (Micromeritics, USA). The specific surface area was calculated with the Brunaue-Emmett-Teller (BET) equation. The pore size and distribution were determined with the Barrett-Joyner-Halenda (BJH) method.

2.4. Adsorption experiment of different ions

An appropriate amount of Na_2CO_3 with a molar ratio of 1.2 times the sum of divalent ions (Ca^{2+}, Mg^{2+}, Ba^{2+}, Sr^{2+}) was added to SGFPW to precipitate these components and eliminate their influence on Li adsorption. The mixture was stirred for 20 minutes at 200 rpm, and let stand for 20 minutes (Jang and Chung, 2018). Finally, the supernatant was drawn for subsequent adsorption experiments. The water quality parameters of SGFPW with or without precipitation pre-treatment are shown in Table S1 (Supporting Information, SI). Adsorption experiments were conducted in both the SGFPW and pre-treated SGFPW (P-SGFPW), and the ion concentration at each step was measured by Dionex Integrion HPIC (Thermo Fisher, USA) after filtration through a membrane with a 0.45 μm pore size.

2.4.1. The effect of pH on extraction of Li^+

The pH values of the SGFPW were controlled in the range of 4 to 11 by 0.1 mol/L of HCl and NaOH. A mass of 0.05 g of the HMO adsorbent was added to 50

mL of SGFPW under different pH values, stirred at 200 rpm for 48 h, and the Li^+ concentration in the supernatant was thus measured. The equilibrium adsorption capacity of Li^+ was calculated according to Eq. (1)

$$q_e = \frac{(C_0 - C_e)V}{m} \quad (1)$$

where q_e (mg/g) is equilibrium adsorption capacity, V (L) is the volume of the solution, m (g) is the weight of HMO adsorbent, C_0 and C_e are the initial and equilibrium Li^+ concentrations in solution (mg/L), respectively.

2.4.2. Adsorption isotherm of Li^+

Different quantities of HMO adsorbents (0.015, 0.025, 0.05, 0.065, 0.075, 0.1 g) were added to 50 mL of the SGFPW or P-SGFPW. The mixture was stirred at 200 rpm for 48 h, and then the Li^+ concentration of the supernatant was determined. The equilibrium adsorption capacity of Li^+ was calculated based on Eq. (1). The Langmuir model and Freundlich model were applied to explore the adsorption mechanism, and details are described in Text S1 (SI).

2.4.3. Adsorption kinetics of Li^+

A mass of 0.05 g of HMO adsorbent was dispersed in 50 mL of the SGFPW or P-SGFPW. The mixed liquid was stirred at 200 rpm for 72 h and the supernatant were taken at regular intervals to measure the concentration of Li^+. The adsorbed amount of lithium at various times was calculated by Eq. (2)

$$q_t = \frac{(C_0 - C_t)V}{m} \quad (2)$$

where q_t (mg/g) and C_t (mg/L) represent the adsorbed amount and the Li^+ concentration in solution at time t, respectively. V (L) is the volume of the solution, *m* (g) is the weight of HMO adsorbent and C_0 is the initial lithium concentration in solution. The pseudo-first-order kinetic model and pseudo-second-order kinetic model were used to investigate the adsorption kinetic behaviors, and the details of the two models are in Text S2 (SI).

2.4.4. Adsorption selectivity of Li^+

In order to compare the adsorption behavior of lithium ions and other metal ions, 0.05 g of adsorbent was added to 50 mL of SGFPW or P-SGFPW and stirred at 200 rpm for 48 h. Metal ion concentrations in the supernatant were then determined, and the partition coefficient (K_d , Eq. (3), concentration factor (CF, Eq. (4), and separation factors (α_{Me}^{Li} , Eq. (5) were calculated to investigate the adsorption selectivity of HMO

$$K_d = \frac{C_0 - C_e}{C_e} \times \frac{V}{m} \tag{3}$$

$$CF = \frac{q_e(Me)}{C_0(Me)} \tag{4}$$

$$\alpha_{Me}^{Li} = \frac{K_d(Li)}{K_d(Me)} \tag{5}$$

where Me represents Li^+, Na^+, K^+, Mg^{2+}, Ca^{2+}, Ba^{2+}, Sr^{2+}. C_0 and C_e are the initial and equilibrium Me concentrations in solution (mg/L), respectively. V (L) is the volume of the solution and *m* (g) is the weight of HMO adsorbent. $q_e(Me)$ (mg/g) and $C_0(Me)$ (mg/L) represent the equilibrium adsorption capacity and initial concentration of Me in solution, respectively.

2.4.5. Reusability study of adsorbents

After each adsorption, the adsorbent was rinsed with ultrapure water, filtered, and dried. Then, it was regenerated with HCl for subsequent adsorption-desorption cycles. The adsorption-desorption cycle was performed four times.

3. Results and discussion

3.1. Characterization of HMO adsorbent

Fig. 1A shows the XRD patterns of the synthesized LMO precursor, its delithiated form HMO, and r-LMO (Li^+-reinserted sample in the P-SGFPW). The XRD patterns of the three samples are almost identical, but there is a slight shift in the positions of the spinel peaks. The XRD pattern of LMO is nearly the same as the standard XRD pattern of $Li_{1.33}Mn_{1.67}O_4$ (PDF No. 46-0810, cubic phase, S.G: Fd3 m (227)), indicating that the LMO precursor was successfully synthesized. The LMO particles show three main diffraction peaks at 2θ = 18.8°, 36.5°, 44.4°, which correspond to the (111), (311), (400) crystal planes of the spinel structure, with crystal face distances (d) of 4.716 Å, 2.460 Å, 2.039 Å, respectively. The main characteristic peaks of HMO were 19.1°, 37°, 45.05°, with crystal face distances (d) of 4.643 Å, 2.428 Å, 2.011 Å, respectively. r-LMO has three main diffraction peaks at 2θ=18.95°, 36.7° and 44.7°, with crystal face distances (d) of 4.679 Å, 2.447 Å, 2.026 Å, respectively. Compared to LMO, the diffraction angle of the HMO was slightly higher, resulting in a decrease in the d-spacing values, indicating that the cell size was reduced, due to the replacement of Li^+ by H^+ with a smaller ion radius (Han et al.,

2012). After adsorption, the diffraction angle of r-LMO decreased again and was practically the same as LMO, indicating that the adsorbent had a stable structure and good cycle performance, and implying the effective ion exchange between H^+ and Li^+.

According to the IUPAC classification (Thommes et al., 2015), the nitrogen adsorption-desorption isotherms of the HMO adsorbent in Fig. 1B is a typical type IV isotherm with an H3 hysteresis loop, indicating that the adsorbent has mesopores. The curve had a distinct uptake of nitrogen adsorption at the relative pressure 0.8-1.0, due to the filling of the mesopores or macropores (Han et al., 2012). The capacity of N_2 adsorption of the HMO adsorbent was 104.7 cm^3/g (STP). The pore size distribution was obtained by calculating the isotherm desorption branch by the BJH method, and the results are shown in Fig. 1C. A bimodal mesoporous structure composed of various mesopore sizes was found, where the small peak indicates a small number of mesopores and the large peak represents the major mesopores with an average pore size of 23-27 nm, which is consistent with the report by Lai et al. (Lai et al., 2020). The BET surface area was 37.8 m^2/g according to the BET surface area plot (Fig. 1D), and the total volume of pores was 0.158 cm^3/g. Fig. 2 shows the SEM images and EDS mapping results of Mn in LMO, HMO, r-LMO samples, indicating similar, hence stable, structures and a uniform distribution on Mn.

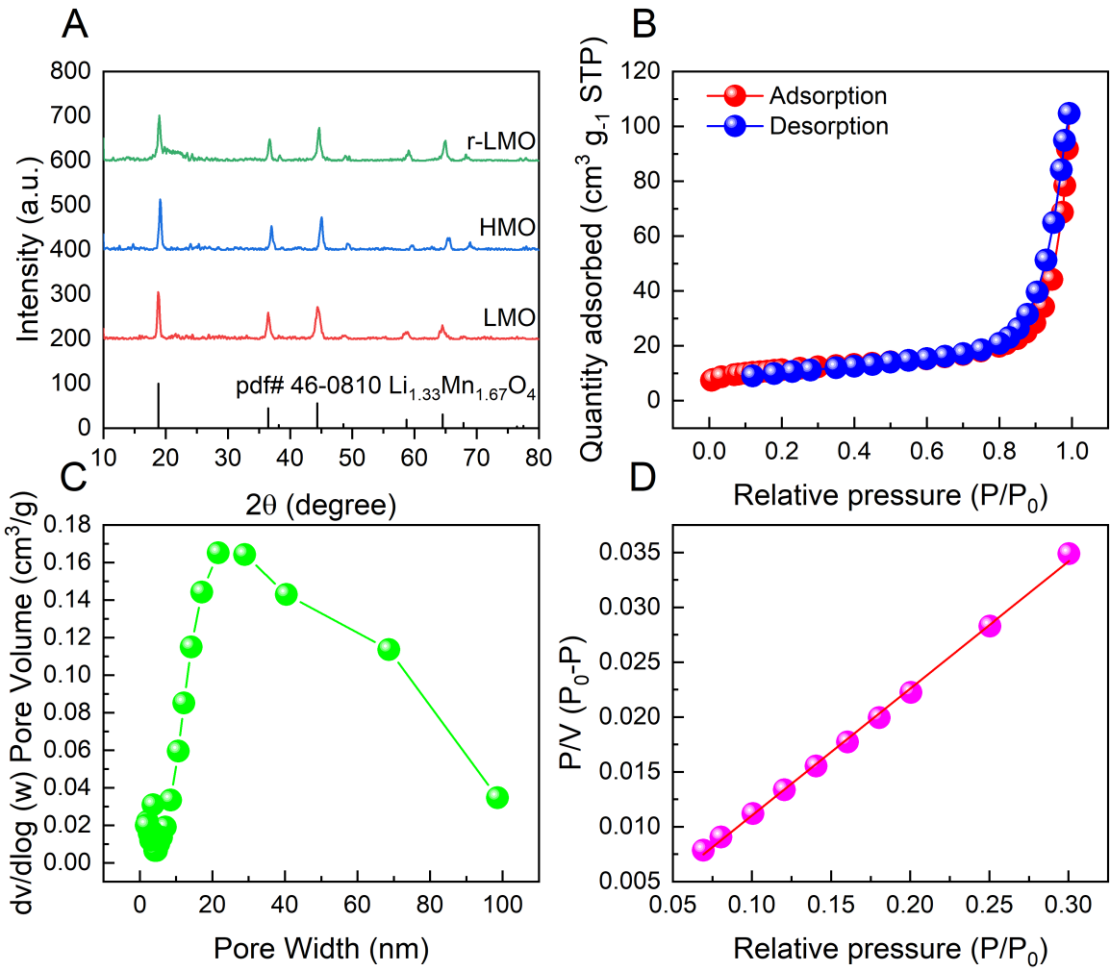

Fig. 1. (A) XRD patterns of the LMO, HMO, and r-LMO. (B) Nitrogen adsorption-desorption isotherms of HMO. (C) Pore size distributions of HMO. (D) BET surface area plot.

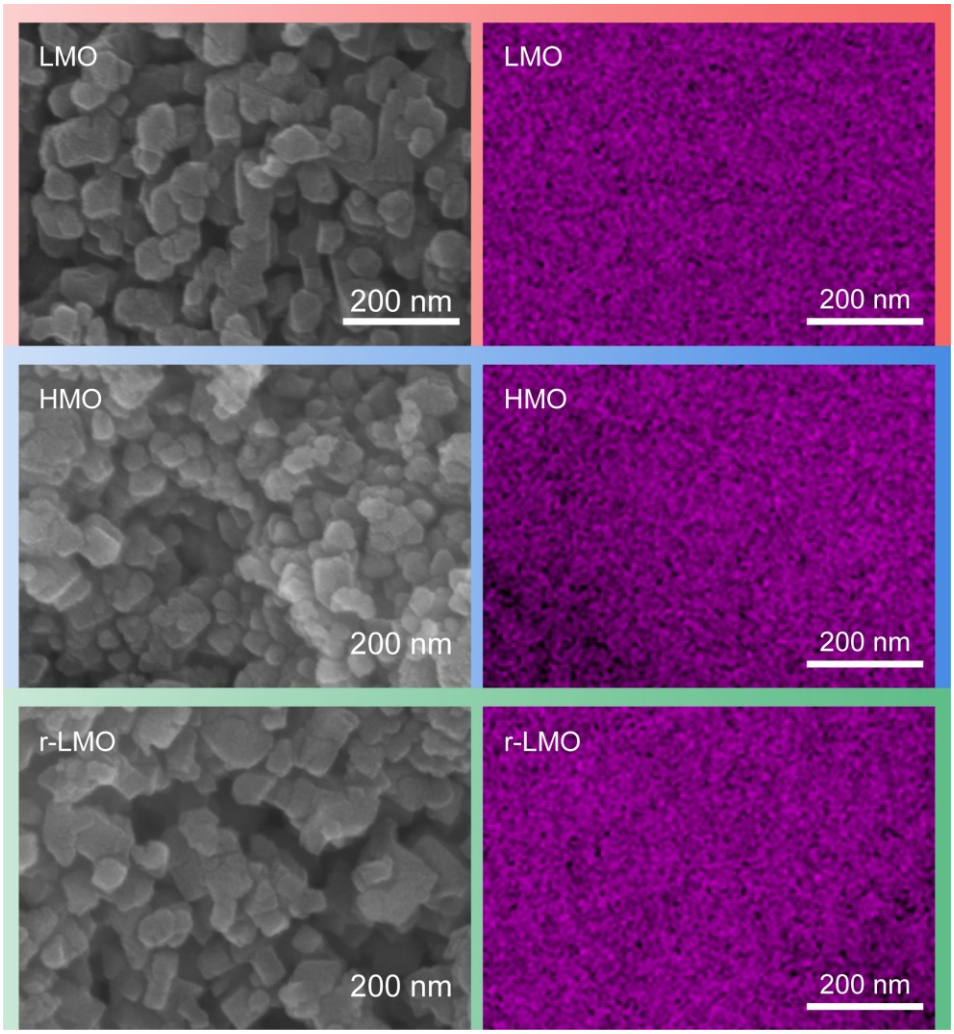

Fig. 2. SEM images and the corresponding EDS mapping results (Mn) of LMO, HMO, r-LMO.

The surface chemistry of LMO, HMO, and r-LMO was analyzed by using X-ray photoelectron spectroscopy. As shown in Fig. 3A, the peaks corresponding to Mn 2p and O 1s were evident, and the peaks corresponding to Mn 3p and Li 1s partially overlapped. Fig. 3B shows the fitting curves of Mn 2p, which were divided into two peaks, Mn 2p1/2 and Mn 2p3/2, with a spin energy separation of 11.2 eV. The O 1s spectra were divided into three peaks including O_{latt} (lattice oxygen), O_{ad} (adsorb

oxygen), and O_{H_2O} (chemisorbed oxygen species) (Luo et al., 2016), as depicted in Fig. 3C. The integral area of the three peaks had a substantial change during the pickling and adsorption process, indicating the change of the chemical environment of the oxygen atom (Qiu et al., 2021). The integral area of HMO was found to be smaller than that of LMO and R-LMO in the Fig. 3D, likely due to the process of ion exchange between H^+ and Li^+, indicating that Li^+ could be successfully adsorbed and desorbed.

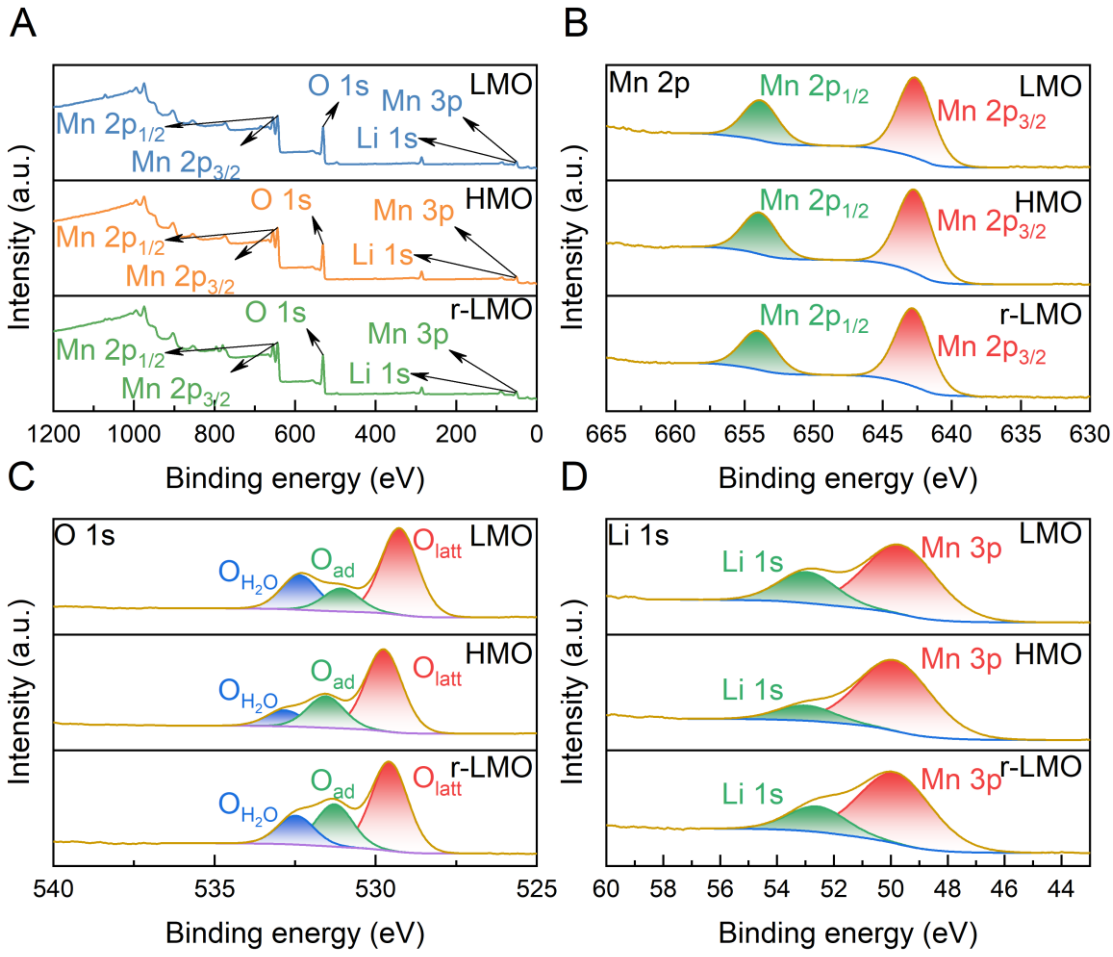

Fig. 3. Analysis of XPS of LMO, HMO, r-LMO. (A) Survey spectra. (B) High resolutions of Mn 2p. (C) High resolutions of O 1s (D) High resolutions of Li 1s.

3.2. Effect of pH on Li^+ adsorption

Th pH values of the solution has a major influence on lithium adsorption capacity because H^+ in acidic solutions will occupy the Li^+ vacancies provided by the HMO adsorbent. The results of experiments assessing the adsorption capacity of lithium at different pH values are shown in Fig 4. The adsorption capacity of lithium increased monotonically with the increase of solution pH. With the increase of pH, the H^+ activity decreases and the competition between H^+ and Li^+ becomes weaker (Qiu et al., 2021; Xu et al., 2019). Also, the surface sites of the HMO adsorbents has a larger density of negative charges as the pH increases (Xiao et al., 2015; Xu et al., 2019), exhibiting stronger affinity for lithium adsorption, which enhance the electrostatic attraction between Li^+ and the adsorbent.

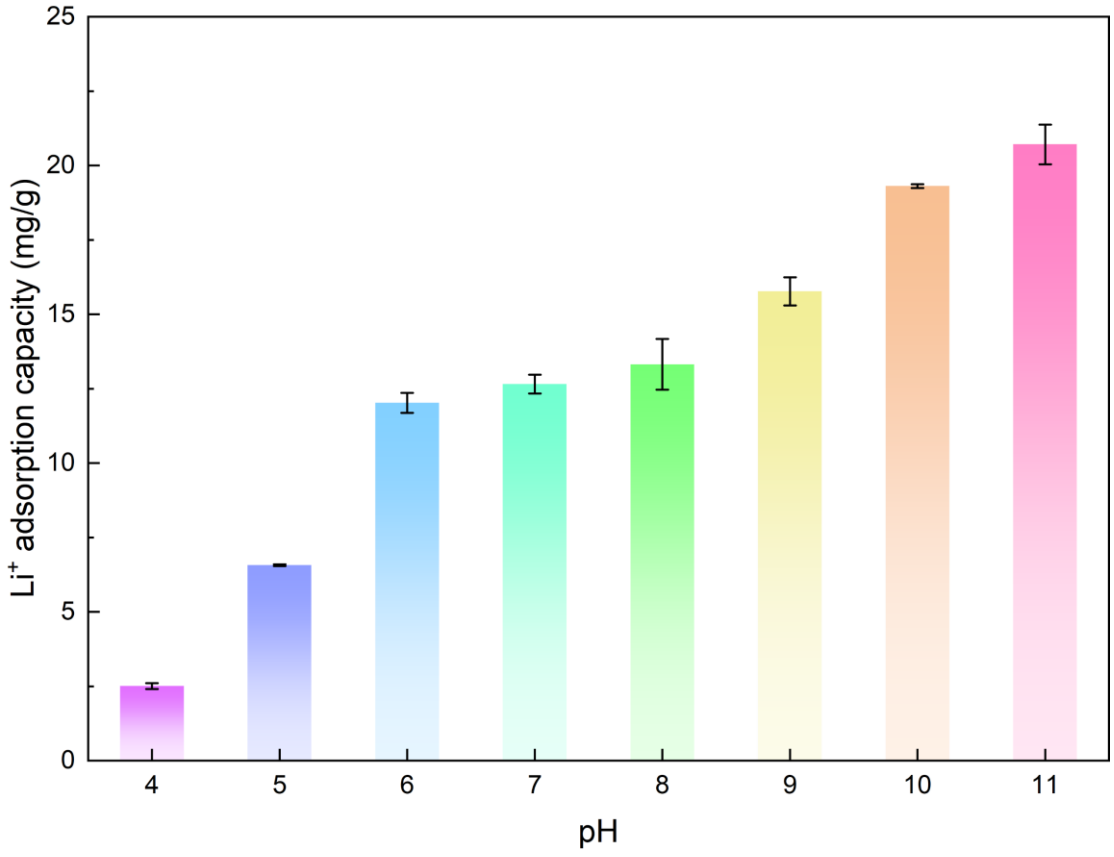

Fig. 4. Lithium adsorption capacity of HMO at different pH values.

3.3. Adsorption isotherms

Adsorption isotherm experiments were performed to investigate the maximum adsorption capacity and the optimal adsorbent dosage. The Langmuir model and Freundlich model are widely used to evaluate the behavior between adsorbates and adsorbents and to study the adsorption mechanism. Fig. 5A and Fig. 5B are the results of fitting the Langmuir model and the Freundlich model to the lithium adsorption isotherm data, respectively. The relevant adsorption isotherm fitting parameters calculated from the two models are summarized in Table 1. The regression coefficients (R^2) of the Langmuir model were higher than those from the Freundlich model for both SGFPW and P-SGFPW, indicating that the Langmuir model described the adsorption isotherms slightly better. This result implies that the adsorption of lithium resembles more closely that of a monolayer chemisorption process that occurs at specific homogeneous sites on the surface of HMO adsorbent (Ryu et al., 2016) and that there was no significant competition between the solvent and sorbate to occupy the sorbent sites (Park et al., 2015). Furthermore, the K_L and the equilibrium adsorption capacity of lithium obtained with P-SGFPW was larger than those observed with SGFPW, suggesting that the precipitation process is advantageous for the adsorption of lithium. The increase in the adsorption capacity of lithium may also be partly due to the increase in pH during Na_2CO_3 precipitation process , from 7.97 to

8.99.

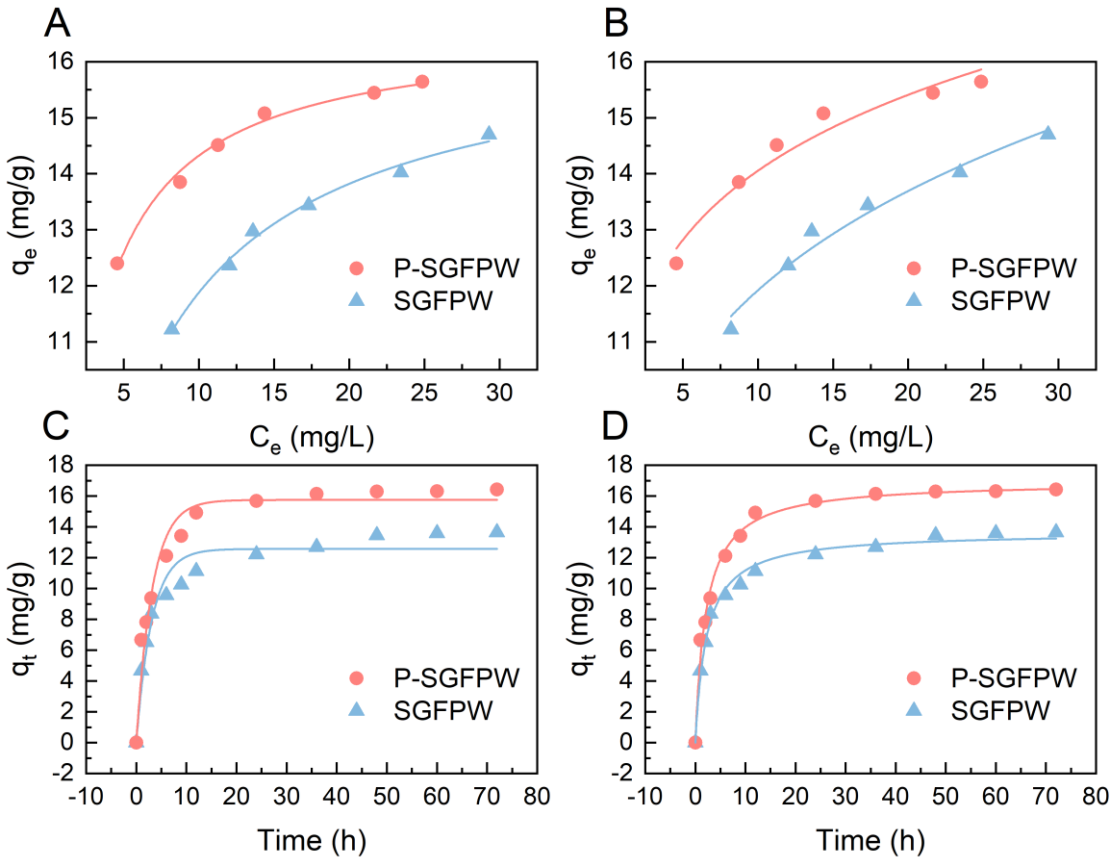

Fig. 5. Adsorption isotherms (A) Langmuir and (B) Freundlich of Li^+ by the HMO adsorbent. Adsorption kinetics (C) pseudo-first-order kinetic model and (D) pseudo-second-order kinetic model of Li^+ by the HMO adsorbent.

Table 1.

Langmuir and Freundlich model fitting parameters of Li^+ adsorption.

	Langmuir model			Freundlich model		
	Q_m (mg/g)	K_L (L/mg)	R^2	K_F ($mg^{1-1/n} \cdot L^{1/n}/g$)	n	R^2
SGFPW	16.52	0.25562	0.9912	7.51	4.99277	0.9762
P-SGFPW	16.61	0.62743	0.9911	10.35	7.52403	0.9492

3.4. Adsorption kinetics

The kinetics of lithium adsorption on HMO adsorbents was studied to comprehend the adsorption behavior and explore the adsorption mechanism, which are important for the construction of reactors, such as fixed-bed reactors, and other fluidized bed operation (Hossain et al., 2022). Kinetic data were fitted using the pseudo-first-order kinetic model and the pseudo-second-order kinetic model, with results displayed in Fig. 5C and Fig. 5D, respectively. It can be seen that lithium is rapidly adsorbed in both SGFPW and P-SGFPW within 6 h and then the adsorption slows down significantly until near-equilibrium was reached after 48 h.. The kinetic parameters reported in Table 2 indicate that the pseudo-second-order kinetics model was slightly more suitable than the pseudo-first-order model. This result implies the adsorption rate is mostly controlled by chemical sorption or chemisorption, likely involving valency forces through exchange of electrons between H^+ and Li^+ (Ho and McKay, 1999). The final experimental adsorption capacities (16.4 mg/g with P-SGFPW) match well the estimated total adsorption capacity (16.9 mg/g with P-SGFPW) based on the pseudo-second-order model, as well as the maximum capacities calculated with Langmuir model for the isotherms (16.6 mg/g with P-SGFPW).

Table 2

Results of fitting the Li^+ adsorption kinetics data with pseudo-first-order model and pseudo-second-order models.

	Pseudo-first-model			Pseudo-second-model		
	$q_{e,cal}$ (mg/g)	k_1 (min^{-1})	R^2	$q_{e,cal}$ (mg/g)	k_2 (g $mg^{-1}h^{-1}$)	R^2
SGFPW	12.57	0.32133	0.9399	13.65	0.03294	0.9905
P-SGFPW	15.75	0.31384	0.9623	16.94	0.02777	0.9913

3.5. Selectivity

SGFPW contains several impurity ions (Na^+, K^+, Mg^{2+}, Ca^{2+}, Ba^{2+}, Sr^{2+}), thus understanding the selectivity of the HMO adsorbents for Li^+ is important. Fig. 6A shows the partition coefficients (K_d) of different ions, while other parameters related to selectivity in the SGFPW and P-SGFPW streams are summarized in Table 3 and Table 4, respectively. The values of K_d for Li^+ in both SGFPW and P-SGFPW were found to be much larger than those of other ions, indicating that Li^+ is more easily adsorbed. Moreover, the coefficient (1074 mL/g) in P-SGFPW was greater than that (731.6 mL/g) in SGFPW, suggesting that precipitation somewhat improved the selectivity to lithium adsorption. The high selectivity is attributed to the ionic sieve effect of the spinel structure of the HMO adsorbent: the adsorption sites are so narrow that only ion with radius smaller than or equal to that of Li^+ can diffuse and be adsorbed (Lai et al., 2020). Although the ionic radius of Mg^{2+} (0.065 nm) is smaller than that of Li^+ (0.068 nm), the hydration free energy of Mg^{2+} (1828 KJ/mol) is nearly four times that of Li^+ (474 KJ/mol), so Mg^{2+} ions need more energy to dehydrate, a necessary step to effectively reach and interact with the adsorption site (Xu et al., 2021). It should be highlighted that the absolute value of the adsorption capacity of Na^+ was also large, which may be due to two main reasons. First, the concentration of Na^+ in solution, which was roughly 400 times that of Li^+ in weight. Likely, Na^+

mostly adsorbed on the outer surface of the adsorbent. While the selectivity of lithium with respect to sodium was high, a significant fraction of adsorption sites are consumed by Na^+, but this effect is inevitable due to the concentration ratio in solution, and in any case less severe than in seawater, whereby the weight-based Na/Li concentration ratio is approximately 200,000, hence 500 times higher than in the SGFPW stream employed in this study. Overall, the HMO adsorbent proved to be a highly selective adsorbent for lithium, especially in pre-treated streams.

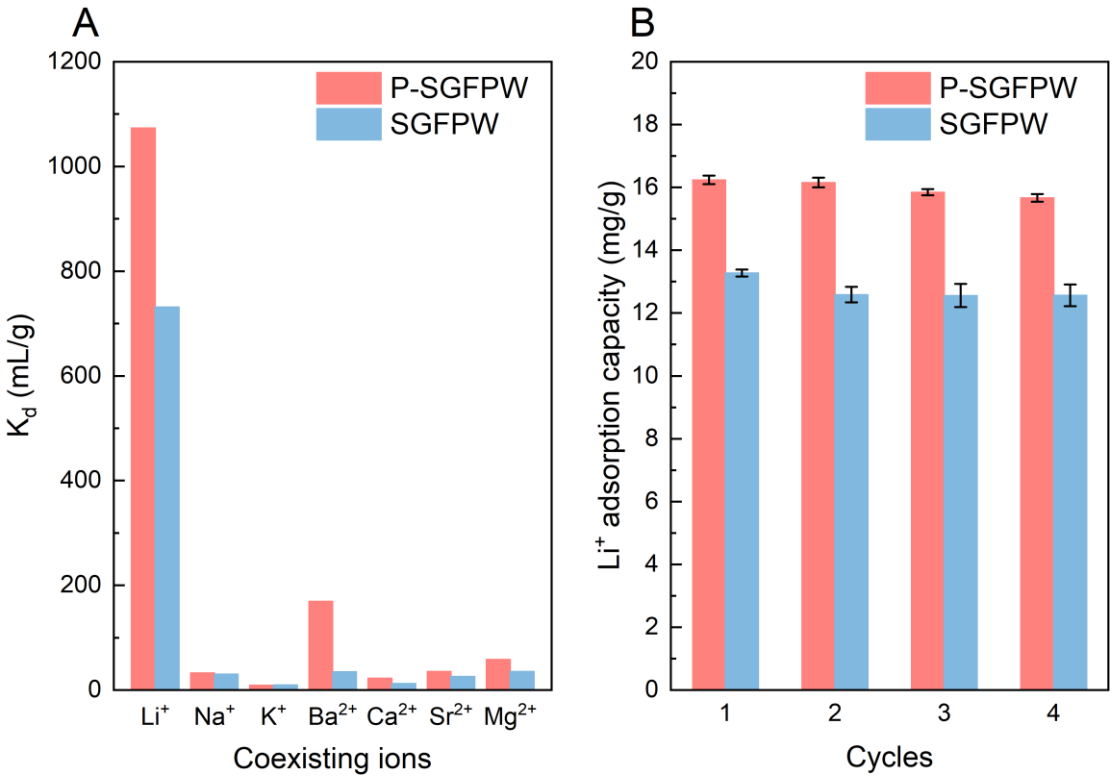

Fig. 6. (A) Partition coefficients (K_d) for coexisting ions. (B) Adsorption capacity of Li^+ at different cycles.

3.6. Reusability of HMO adsorbent

A good adsorbent should have a stable structure and excellent reusability, which

helps reducing the cost of the adsorption process. The reusability of the HMO adsorbent was evaluated through four adsorption-desorption cycles, and the adsorption capacity of Li^+ in each cycle is shown in Fig. 6B. The adsorption capacity was relatively stable with only a slight decrease after each regeneration, and it decreased from 16.2 to 15.7 mg/g and from 13.3 to 12.6 mg/g in P-SGFPW and SGFPW, respectively, after four cycles. This phenomenon may be due to the fact that HMO adsorbent has excellent crystallization properties, which is consistent with the XRD results. These results suggest that the HMO adsorbent can be reused in SGFPW and is a promising adsorbent for lithium recovery from SGFPW.

Table 3

Adsorption selectivity of HMO in the SGFPW.

	C_0 (mg/L)	C_e (mg/L)	q_e (mg/g)	K_d (ml/g)	CF (ml/g)	α_{Me}^{Li}
Li^+	31.46	18.15	13.27	731.58	421.94	1
Na^+	12122.22	11765.40	355.51	30.22	29.33	24.21
K^+	282.40	279.71	2.69	9.60	9.51	79.20
Ba^{2+}	116.45	112.51	3.92	34.85	33.67	20.99
Ca^{2+}	523.12	516.74	6.35	12.30	12.15	59.49
Sr^{2+}	104.25	101.64	2.60	25.54	24.90	28.64
Mg^{2+}	74.17	71.64	2.52	35.23	34.03	20.77

Table 4

Adsorption selectivity of HMO in the P-SGFPW.

	C_0 (mg/L)	C_e (mg/L)	q_e (mg/g)	K_d (ml/g)	CF (ml/g)	α_{Me}^{Li}
Li^+	31.40	15.13	16.24	1073.58	517.23	1
Na^+	13115.89	12704.55	410.50	32.31	31.30	33.23
K^+	281.45	278.99	2.46	8.83	8.76	121.52
Ba^{2+}	12.07	10.32	1.75	169.24	144.70	6.34
Ca^{2+}	43.35	42.39	0.96	22.63	22.13	47.44

Sr^{2+}	37.27	36.00	1.27	35.16	33.96	30.53
Mg^{2+}	62.90	59.43	3.47	58.38	55.15	18.39

4. Conclusion

$H_{1.33}Mn_{1.67}O_4$ (HMO) adsorbent was synthesized by solid-phase reaction method and applied in the raw and pre-treated shale gas flowback and produced water (SGFPW and P-SGFPW, respectively). The adsorption capacity of lithium increased monotonically with the increase of pH in the range of 4 to 11. The lithium adsorption properties of the HMO adsorbent in both SGFPW and P-SGFPW matched well with the pseudo-second-order kinetic model and with the Langmuir equilibrium model, suggesting that the adsorption of lithium is likely a substitution process between H^+ and Li^+ and that the rate-limiting step may be chemical sorption. According to the adsorption isotherm analysis of lithium, the equilibrium adsorption capacity of lithium in the P-SGFPW was larger than that in the SGFPW. Due to the larger ionic radius and higher free energy of hydration, the HMO adsorbent has high selectivity to lithium, especially after the wastewater was pre-treated by precipitation. The partition coefficient of Li^+ (1074mL/g) was much larger than that of Ba (169.24 mL/g), Mg (58.4 mL/g), Sr (35.2 mL/g), Na (32.3 mL/g), Ca (22.6 mL/g), K (8.83 mL/g). After four adsorption-desorption cycles, the adsorption capacity of lithium in P-SGFPW decreased from 16.2 mg/g to 15.7 mg/g, indicating that the HMO adsorbent had a stable structure and good reusability. However, it should be highlighted that the HMO adsorbent powder had poor dispersibility in aqueous suspension and its recovery may

be challenging during operation. Therefore, the granulation of powder HMO adsorbent would be important to promote its practical application.

Supporting Information

The Supporting Information is available free of charge online.

Acknowledgments

This work was supported by the National Natural Science Foundation of China (52070134), Litree Purifying Technology Co., Ltd. Project (2021H012), and Sichuan University and Yibin City People's Government strategic cooperation project (2020CDYB-2). The views and ideas expressed herein are solely those of the authors and do not represent the ideas of the funding agencies in any form.

References

Bunani, S., Arda, M., Kabay, N., Yoshizuka, K. and Nishihama, S. , 2017. Effect of process conditions on recovery of lithium and boron from water using bipolar membrane electrodialysis (BMED). Desalination 416, 10-15.

Chan, K.H., Malik, M. and Azimi, G. , 2022. Separation of lithium, nickel, manganese, and cobalt from waste lithium-ion batteries using electrodialysis. Resour., Conserv. Recycl. 178, 106076.

Chen, J., Lin, S. and Yu, J. , 2020. Quantitative effects of Fe_3O_4 nanoparticle content on Li^+ adsorption and magnetic recovery performances of magnetic lithium-aluminum layered double hydroxides in ultrahigh Mg/Li ratio brines. J. Hazard. Mater. 388, 122101.

Draaisma, D. , 2019. Lithium: the gripping history of a psychiatric success story. Nature 572(7771), 584-585.

Haluszczak, L.O., Rose, A.W. and Kump, L.R. , 2013. Geochemical evaluation of flowback brine from Marcellus gas wells in Pennsylvania, USA. Appl. Geochem. 28, 55-61.

Han, Y., Kim, H. and Park, J. , 2012. Millimeter-sized spherical ion-sieve foams with hierarchical pore structure for recovery of lithium from seawater. Chem. Eng. J. 210, 482-489.

Han, Y., Kim, S., Yu, S., Myung, N.V. and Kim, H. , 2020. Electrospun hydrogen manganese oxide nanofibers as effective adsorbents for Li^+ recovery from

seawater. J. Ind. Eng. Chem. 81, 115-123.
Ho, Y.S. and McKay, G. , 1999. Pseudo-second order model for sorption processes. Process Biochem. 34(5), 451-465.
Hossain, S.M., Ibrahim, I., Choo, Y., Razmjou, A., Naidu, G., Tijing, L., Kim, J.-H. and Shon, H.K. , 2022. Preparation of effective lithium-ion sieve from sludge-generated TiO_2. Desalination 525, 115491.
Hou, J., Zhang, H., Thornton, A.W., Hill, A.J., Wang, H. and Konstas, K. , 2021. Lithium Extraction by Emerging Metal–Organic Framework-Based Membranes. Adv. Funct. Mate. 31(46), 2105991.
Jang, Y. and Chung, E. , 2018. Adsorption of Lithium from Shale Gas Produced Water Using Titanium Based Adsorbent. Ind. Eng. Chem. Res. 57(25), 8381-8387.
Jang, Y., Hou, C.-H., Park, S., Kwon, K. and Chung, E. , 2021. Direct electrochemical lithium recovery from acidic lithium-ion battery leachate using intercalation electrodes. Resour., Conserv. Recycl. 175, 105837.
Ji, Z.-Y., Zhao, M.-Y., Zhao, Y.-Y., Liu, J., Peng, J.-L. and Yuan, J.-S. , 2017. Lithium extraction process on spinel-type $LiMn_2O_4$ and characterization based on the hydrolysis of sodium persulfate. Solid State Ionics 301, 116-124.
Kondash, A.J., Lauer, N.E. and Vengosh, A. , 2018. The intensification of the water footprint of hydraulic fracturing. Sci. Adv. 4(8), eaar5982.
Kumar, A., Fukuda, H., Hatton, T.A. and Lienhard, J.H. , 2019. Lithium Recovery from Oil and Gas Produced Water: A Need for a Growing Energy Industry. ACS Energy Lett. 4(6), 1471-1474.
Lai, X.R., Yuan, Y.J., Chen, Z.Q., Peng, J.H., Sun, H. and Zhong, H. , 2020. Adsorption-Desorption Properties of Granular EP/HMO Composite and Its Application in Lithium Recovery from Brine. Ind. Eng. Chem. Res. 59(16), 7913-7925.
Lawagon, C.P., Nisola, G.M., Cuevas, R.A.I., Kim, H., Lee, S.P. and Chung, W.J. ,2019. Development of high capacity Li+ adsorbents from H_2TiO_3/polymer nanofiber composites: Systematic polymer screening, characterization and evaluation. J. Ind. Eng. Chem. 70, 124-135.
Liu, Y., Wu, Q., Chen, C., Li, T., Liu, S., He, Q., Yang, P., Bai, Y. and Liu, B. , 2022. An efficient system of aerogel adsorbent combin`ed with membranes for reuse of shale gas wastewater. Desalination 526, 115545.
Luo, X., Zhang, K., Luo, J., Luo, S. and Crittenden, J. , 2016. Capturing Lithium from Wastewater Using a Fixed Bed Packed with 3-D MnO_2 Ion Cages. Environ. Sci. Technol. 50(23), 13002-13012.
Miatto, A., Wolfram, P., Reck, B.K. and Graedel, T.E. , 2021. Uncertain Future of American Lithium: A Perspective until 2050. Environ. Sci. Technol. 55(23), 16184-16194.
Park, H., Singhal, N. and Jho, E.H. , 2015. Lithium sorption properties of HMnO in seawater and wastewater. Water Res. 87, 320-327.
Pramanik, B.K., Asif, M.B., Kentish, S., Nghiem, L.D. and Hai, F.I. , 2019. Lithium

enrichment from a simulated salt lake brine using an integrated nanofiltration-membrane distillation process. J. Environ. Chem. Eng. 7(5), 103395.

Qiu, Y., Ruan, H., Tang, C., Yao, L., Shen, J. and Sotto, A. , 2019. Study on Recovering High-Concentration Lithium Salt from Lithium-Containing Wastewater Using a Hybrid Reverse Osmosis (RO)–Electrodialysis (ED) Process. ACS Sustainable Chem. Eng. 7(15), 13481-13490.

Qiu, Z.W., Wang, M.Y., Chen, Y., Zhang, T., Yang, D.Y. and Qiu, F.X. , 2021. $Li_4Mn_5O_{12}$ doped cellulose acetate membrane with low Mn loss and high stability for enhancing lithium extraction from seawater. Desalination 506, 115003.

Robbins, C.A., Du, X., Bradley, T.H., Quinn, J.C., Bandhauer, T.M., Conrad, S.A., Carlson, K.H. and Tong, T. , 2022. Beyond treatment technology: Understanding motivations and barriers for wastewater treatment and reuse in unconventional energy production. Resour., Conserv. Recycl. 177, 106011.

Ryu, T., Haldorai, Y., Rengaraj, A., Shin, J., Hong, H.-J., Lee, G.-W., Han, Y.-K., Huh, Y.S. and Chung, K.-S. , 2016. Recovery of Lithium Ions from Seawater Using a Continuous Flow Adsorption Column Packed with Granulated Chitosan–Lithium Manganese Oxide. Ind. Eng. Chem. Res. 55(26), 7218-7225.

Safari, S., Lottermoser, B.G. and Alessi, D.S. , 2020. Metal oxide sorbents for the sustainable recovery of lithium from unconventional resources. Appl. Mater. Today 19, 100638.

Scrosati, B., Hassoun, J. and Sun, Y.-K. , 2011. Lithium-ion batteries. A look into the future. Energy Environ. Sci. 4(9), 3287-3295.

Seip, A., Safari, S., Pickup, D.M., Chadwick, A.V., Ramos, S., Velasco, C.A., Cerrato, J.M. and Alessi, D.S. , 2021. Lithium recovery from hydraulic fracturing flowback and produced water using a selective ion exchange sorbent. Chem. Eng. J. 426, 130713.

Shi, W., Liu, X., Ye, C., Cao, X., Gao, C. and Shen, J. , 2019. Efficient lithium extraction by membrane capacitive deionization incorporated with monovalent selective cation exchange membrane. Sep. Purif. Technol. 210, 885-890.

Su, Y., Qian, F. and Qian, Z. , 2022. Enhancing adsorption capacity and structural stability of $Li_{1.6}Mn_{1.6}O_4$ adsorbents by anion/cation co-doping. RSC Adv. 12(4), 2150-2159.

Sun, Y., Wang, Q., Wang, Y., Yun, R. and Xiang, X. , 2021. Recent advances in magnesium/lithium separation and lithium extraction technologies from salt lake brine. Sep. Purif. Technol. 256, 117807.

Sutijan, S., Wahyudi, S., Ismail, M.F., mustika, P.C.B., Astuti, W., Prasetya, A. and Petrus, H.T.B.M. , 2022. Forward Osmosis to Concentrate Lithium from Brine: The Effect of Operating Conditions (pH and Temperature). Int. J. Technol. 13(1), 291-319.

Swain, B. , 2017. Recovery and recycling of lithium: A review. Sep. Purif. Technol. 172, 388-403.

Tang, L., Huang, S., Wang, Y., Liang, D., Li, Y., Li, J., Wang, Y., Xie, Y. and Wang, W. , 2020. Highly Efficient, Stable, and Recyclable Hydrogen Manganese Oxide/Cellulose Film for the Extraction of Lithium from Seawater. ACS Appl. Mater. Interfaces 12(8), 9775-9781.

Tang, P., Liu, B., Xie, W., Wang, P., He, Q., Bao, J., Zhang, Y., Zhang, Z., Li, J. and Ma, J. , 2022. Synergistic mechanism of combined ferrate and ultrafiltration process for shale gas wastewater treatment. J. Membrane Sci. 641, 119921.

Tarascon, J.-M. , 2010. Is lithium the new gold? Nat. Chem. 2(6), 510-510.

Thommes, M., Kaneko, K., Neimark, A.V., Olivier, J.P., Rodriguez-Reinoso, F., Rouquerol, J. and Sing, K.S.W. , 2015. Physisorption of gases, with special reference to the evaluation of surface area and pore size distribution (IUPAC Technical Report). Pure Appl. Chem. 87(9-10), 1051-1069.

Tian, L., Chang, H., Tang, P., Li, T., Zhang, X., Liu, S., He, Q., Wang, T., Yang, J., Bai, Y., Vidic, R.D., Crittenden, J.C. and Liu, B. , 2020. Rare Earth Elements Occurrence and Economical Recovery Strategy from Shale Gas Wastewater in the Sichuan Basin, China. ACS Sustainable Chem. Eng. 8(32), 11914-11920.

U. S. Geological Survey, 2012. Mineral Commodity Summaries 2012: U. S. Geological Survey, 198p.

U. S. Geological Survey, 2022. Mineral Commodity Summaries 2022: U. S. Geological Survey, 202p.

Wang, L., Rehman, D., Sun, P.-F., Deshmukh, A., Zhang, L., Han, Q., Yang, Z., Wang, Z., Park, H.-D., Lienhard, J.H. and Tang, C.Y. , 2021. Novel Positively Charged Metal-Coordinated Nanofiltration Membrane for Lithium Recovery. ACS Appl. Mater. Interfaces 13(14), 16906-16915.

Xiao, J., Nie, X., Sun, S., Song, X., Li, P. and Yu, J. , 2015. Lithium ion adsorption–desorption properties on spinel $Li_4Mn_5O_{12}$ and pH-dependent ion-exchange model. Adv. Powder Technol. 26(2), 589-594.

Xie, J. and Lu, Y.-C. , 2020. A retrospective on lithium-ion batteries. Nat. Commun. 11(1), 2499.

Xie, W., Tang, P., Wu, Q., Chen, C., Song, Z., Li, T., Bai, Y., Lin, S., Tiraferri, A. and Liu, B. , 2022. Solar-driven desalination and resource recovery of shale gas wastewater by on-site interfacial evaporation. Chem. Eng. J. 428, 132624.

Xiong, Y., Ge, T., Xu, L., Wang, L., He, J., Zhou, X., Tian, Y. and Zhao, Z. , 2022. A fundamental study on selective extraction of Li^+ with dibenzo-14-crown-4 ether: Toward new technology development for lithium recovery from brines. J. Environ. Manage. 310, 114705.

Xu, N.C., Li, S.X., Guo, M., Qian, Z.Q., Li, W. and Liu, Z. , 2019. Synthesis of $H_4Mn_5O_{12}$ Nanotubes Lithium Ion Sieve and Its Adsorption Properties for Li^+ from Aqueous Solution. Chemistryselect 4(33), 9562-9569.

Xu, S., Song, J., Bi, Q., Chen, Q., Zhang, W.-M., Qian, Z., Zhang, L., Xu, S., Tang, N. and He, T. , 2021. Extraction of lithium from Chinese salt-lake brines by membranes: Design and practice. J. Membrane Sci. 635, 119441.

Yang, S., Zhang, F., Ding, H., He, P. and Zhou, H. , 2018. Lithium Metal Extraction from Seawater. Joule 2(9), 1648-1651.

Zhang, G., Zhang, J., Zhou, Y., Qi, G., Zeng, J., Sun, Y., Shen, Y., Li, X., Ren, X., Dong, S., Sun, C., Wu, Z., Hai, C. and Tang, W. , 2021a. Practical synthesis of manganese oxide $MnO_2 \cdot 0.5H_2O$ for an advanced and applicable lithium ion-sieve. J. Solid State Chem. 293.

Zhang, S., Wang, Z., Chen, C., Jia, J. and Chen, Z. , 2021b. Pressure wave behavior and its effects on structure under In-box LOCA in a helium-cooled lead lithium blanket of hydrogen fusion reactors. Int. J. Hydrogen Energ. 46(10), 7415-7425.

Zhang, Y., Hu, Y., Sun, N., Khoso, S.A., Wang, L. and Sun, W. , 2019. A novel precipitant for separating lithium from magnesium in high Mg/Li ratio brine. Hydrometallurgy 187, 125-133.

Zhao, B., Qian, Z., Guo, M., Wu, Z. and Liu, Z. , 2021. The performance and mechanism of recovering lithium on $H_4Ti_5O_{12}$ adsorbents influenced by (1 1 0) and (1 1 1) facets exposed. Chem. Eng. J. 414.

Zhong, J., Lin, S. and Yu, J. , 2021. Lithium recovery from ultrahigh Mg^{2+}/Li^{+} ratio brine using a novel granulated Li/Al-LDHs adsorbent. Sep. Purif. Technol. 256.

Zhu, X., Yue, H., Sun, W., Zhang, L., Cui, Q. and Wang, H. , 2021. Study on adsorption extraction process of lithium ion from West Taijinar brine by shaped titanium-based lithium ion sieves. Sep. Purif. Technol. 119099.

Graphical Abstract